Nanoscale

Synthesis of active, robust and cationic Au_{25} cluster catalysts on double metal hydroxide by long-term oxidative aging of $Au_{25}(SR)_{18}$

Journal:	*Nanoscale*
Manuscript ID	NR-ART-11-2021-007493.R1
Article Type:	Paper
Date Submitted by the Author:	11-Dec-2021
Complete List of Authors:	Masuda, Shinya; The University of Tokyo, Department of Chemistry, School of Science Takano, Shinjiro; The University of Tokyo, Department of Chemistry, Graduate School of Science Yamazoe, Seiji; Tokyo Metropolitan University, Department of Chemistry; Kyoto University, Elements Strategy Initiative for Catalysts and Batteries (ESICB) Tsukuda, Tatsuya; The University of Tokyo, Department of Chemistry, School of Science; Kyoto University, Elements Strategy Initiative for Catalysts and Batteries (ESICB)

ARTICLE

Synthesis of active, robust and cationic Au_{25} cluster catalysts on double metal hydroxide by long-term oxidative aging of $Au_{25}(SR)_{18}$

Received 00th January 20xx,
Accepted 00th January 20xx

DOI: 10.1039/x0xx00000x

Shinya Masuda [a], Shinjiro Takano [a], Seiji Yamazoe [b, c], and Tatsuya Tsukuda*[a, c]

Synthesis of an atomically precise Au_{25} cluster catalyst was attempted by long-term, low-temperature pretreatment of $Au_{25}(BaET)_{18}$ (BaET-H = 2-(Boc-amino)ethanethiol) on various double metal hydroxide (DMH) supports. X-ray absorption fine structure analysis revealed that bare Au_{25} clusters with high loading (1 wt%) were successfully generated on the DMH containing Co and Ce (Co_3Ce) by oxidative aging in air at 150 °C for >12 h. X-ray absorption near-edge structure and X-ray photoelectron spectroscopies showed that the Au_{25} clusters on Co_3Ce were positively charged. The Au_{25}/Co_3Ce catalyst thus synthesized exhibited superior catalytic performance (TOF = 1097 h^{-1} with >97% selectivity to benzoic acid) in the aerobic oxidation of benzyl alcohol under ambient conditions and high durability owing to a strong anchoring effect. Based on kinetic experiments, we propose that abstraction of hydride from α-carbon of benzyl alkoxide by Au_{25} is the rate-determining step of benzyl alcohol oxidation by Au_{25}/Co_3Ce.

Introduction

Since Haruta's discovery of catalysis by small gold nanoparticles (AuNPs) for CO oxidation,[1] the origin of the size-specific catalysis by AuNPs has been one of the central issues in nanoscience.[2-5] Previous extensive studies have revealed that the catalytic activity of AuNPs was enhanced by reducing the diameter[6] and by using reducible metal oxides or basic supports.[7-10] After decades of controversy, the research community has reached a consensus that the perimeter region between the AuNP and the support provides an active site for CO oxidation.[7, 8, 11, 12] It is proposed that O atoms formed by dissociative adsorption of O_2 at the interface react with CO adsorbed on AuNP to generate CO_2.[8] Thus, the AuNP is not directly involved in activation of CO and O_2, but provides an activation site for O_2 at the interface with the support.

In contrast, Au clusters smaller than ~2 nm in diameter are expected to directly activate small molecules owing to nonmetallic, quantized electronic structures.[13-17] It was demonstrated that free Au_n^- anions isolated in the gas phase and Au_n ($n \geq 8$) clusters soft-landed on TiO_2 exhibited size-specific and size-dependent catalysis for CO oxidation via reductive activation of O_2.[18-20] Thus, heterogeneous Au cluster catalysts (AuCCs) with atomically precise sizes may exhibit novel and superior catalysis as well as provide ideal platforms for investigating the origin of the catalysis.[21] However, atomically precise synthesis of heterogeneous AuCCs cannot be achieved by the conventional methods, such as co-precipitation and impregnation. One of the promising approaches is to adsorb atomically-defined Au clusters fully protected by ligands onto a solid support and to pretreat these precursors for catalytic application (**Scheme 1**).[22] The most conventional pretreatment is removal of the ligands by calcination in vacuum.[23-34] For example, thiolates (RS^-) are desorbed from $Au_x(SR)_y$ by heating them at a temperature (>250 °C) higher than that required for the powder form of $Au_x(SR)_y$ (~200 °C).[27-34] The desorption processes and the structures of the resulting clusters have been studied intensively using a variety of methods including thermogravimetric analysis, mass spectrometry, transmission electron microscopy (TEM), theoretical calculation, and X-ray absorption spectroscopy (XAS). One of the limitations of this approach is that the density of supported clusters has to be suppressed (<0.2 wt% loading and/or use of supports with high surface area) to avoid thermal-induced aggregation/dissociation of the clusters (**Scheme 1**).[35, 36] Such low loading hampers detailed structural characterization of the AuCCs using X-ray photoelectron spectroscopy (XPS), for example. Another pretreatment method of $Au_x(SR)_y$ reported so far includes aging at a low temperature (~150 °C) in the presence of oxygen.[23, 25] This oxidative aging is expected to overcome the problems encountered in high-temperature calcination: the loading can be enhanced without aggregation since a majority of the thiolates still remain on the cluster surface. However, much less is known about the structural change of the clusters during oxidative aging than in the case of calcination (**Scheme 1**).

[a] Department of Chemistry, Graduate School of Science, The University of Tokyo, 7-3-1 Hongo, Bunkyo-ku, Tokyo 113-0033, Japan.
[b] Department of Chemistry, Graduate School of Science, Tokyo Metropolitan University, 1-1 Minami-Osawa, Hachioji-shi, Tokyo 192-0397, Japan.
[c] Elements Strategy Initiative for Catalysts and Batteries (ESICB), Kyoto University, Katsura, Kyoto 615-8520, Japan.
† Footnotes relating to the title and/or authors should appear here.
Electronic Supplementary Information (ESI) available: [details of any supplementary information available should be included here]. See DOI: 10.1039/x0xx00000x

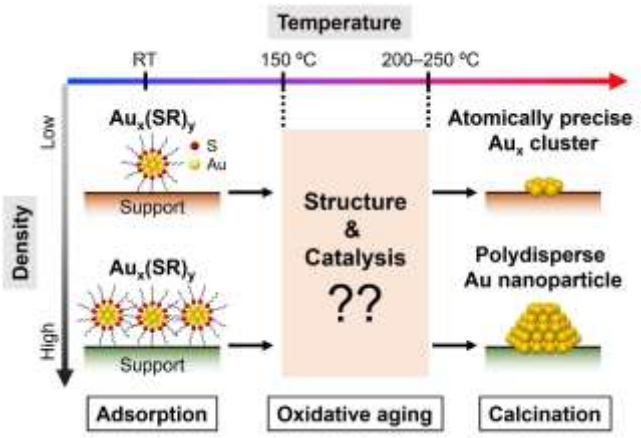

Scheme 1 Pretreatment of thiolate-protected Au clusters for catalytic application.

Motivated by these reports, we focused on the structural change of $Au_x(SR)_y$ during long-term oxidative aging at low temperature and the catalytic properties of the resulting structures. As the precursor, we chose the representative $Au_{25}(SR)_{18}$, which has an icosahedral Au_{13} core protected by six $Au_2(SR)_3$ bidentate oligomers.[37] As supports, we chose (layered) double metal hydroxides (DMHs) composed of Al^{3+} or Ce^{3+} as a trivalent metal cation and Mg^{2+}, Ni^{2+} or Co^{2+} as a divalent metal cation due to the following reasons: (i) they show unique basic and redox properties;[31, 32, 38-40] (ii) small AuNPs supported on layered double hydroxides (LDHs) exhibited high activity in alcohol oxidation;[38, 39] and (iii) Au_x/LDH prepared by calcination of 0.2 wt% $Au_x(Capt)_y$ (Capt-H = captopril) at high temperature (~300 °C) exhibited high activity in the base-free alcohol oxidation.[31, 32] In this work, various $Au_{25}(SR)_{18}$ supported on LDH/DMH were aged under an oxidative atmosphere (**Scheme 2**) for as long as 30 h. The structures were thoroughly characterized by Au L_3-edge X-ray absorption fine structure (XAFS) analysis. We found that the RS ligands were completely removed by aging of $Au_{25}(SR)_{18}$ on Co_3Ce for ≥ 12 h at a surprisingly low temperature (150 °C). Au L_3-edge X-ray absorption near-edge structure (XANES) analysis and XPS revealed that cationic bare Au_{25} clusters were formed on Co_3Ce through the formation of Au–O bonds even at the loading of as high as 1 wt%. The Au_{25}/Co_3Ce catalyst thus prepared exhibited significantly high catalytic activity in the aqueous phase oxidation of benzyl alcohol under ambient conditions. Based on kinetic experiments, we propose that abstraction of hydride from α-carbon of benzyl alkoxide by Au_{25} corresponds to the rate-determining step (RDS) of benzyl alcohol oxidation by Au_{25}/Co_3Ce. This work provides a new avenue for the development of atomically precise heterogeneous AuCCs for various types of reactions.

Results and discussion

Synthesis and characterization of Au_{25}/DMH catalysts

The Au_{25} clusters supported on DMHs were synthesized in three steps: (1) synthesis of $Au_{25}(SR)_{18}$; (2) synthesis of DMHs; and (3) oxidative aging of $Au_{25}(SR)_{18}$ on DMHs (**Scheme 2**). Details of each step are described in the following (see Supplementary Information for details).

Firstly, $Au_{25}(PET)_{18}^{-/0}$ (PET-H = 2-phenylethanethiol) and $Au_{25}(Capt)_{18}^-$ were synthesized according to the reported method.[41, 42] $Au_{25}(BaET)_{18}^-$ (BaET-H = 2-(Boc-amino)ethanethiol) was synthesized by the ligand exchange of $Au_{25}(PET)_{18}^-$ (**Scheme 2**). Electrospray ionization (ESI) mass spectra (**Fig. 1A**) showed that $Au_{25}(PET)_{18}^-$ and $Au_{25}(BaET)_{18}^-$ were obtained in a pure form. The matrix-assisted laser desorption/ionization (MALDI) mass spectrum of $Au_{25}(PET)_{18}^0$ suggested the formation of the desired product (**Fig. 1B**). The UV-vis absorption spectra of the toluene solutions of $Au_{25}(PET)_{18}^0$, $Au_{25}(PET)_{18}^-$ and $Au_{25}(BaET)_{18}^-$, and the methanol (MeOH) solution of $Au_{25}(Capt)_{18}^-$ (**Fig. 1C**) agreed well with those reported in the literature. The $Au_{25}(BaET)_{18}^-$ sample was further characterized by thermogravimetric (TG) analysis (**Fig. 1D**). The ligand desorption started at ~175 °C and the weight loss after complete desorption was 39.7 wt%, which agreed well with the theoretical calculated value (39.2 wt%). These results confirmed that desired clusters were successfully obtained in a molecularly pure form.

Secondly, various DMH supports were prepared by the conventional co-precipitation method in basic aqueous solutions (**Scheme 2**).[32] **Fig. 1E** and **1F** show PXRD patterns of DMHs containing Al^{3+} and Ce^{3+}, respectively. The Al^{3+}-containing DMHs showed similar PXRD patterns with that of reference Mg_3Al-LDH, although Co_3Al has lower crystallinity than Mg_3Al and Ni_3Al (**Fig. 1E**). Two Ce^{3+}-containing DMHs, Ni_3Ce and Co_3Ce, had higher crystallinity than Mg_3Ce (**Fig. 1F**). The Co_3Ce

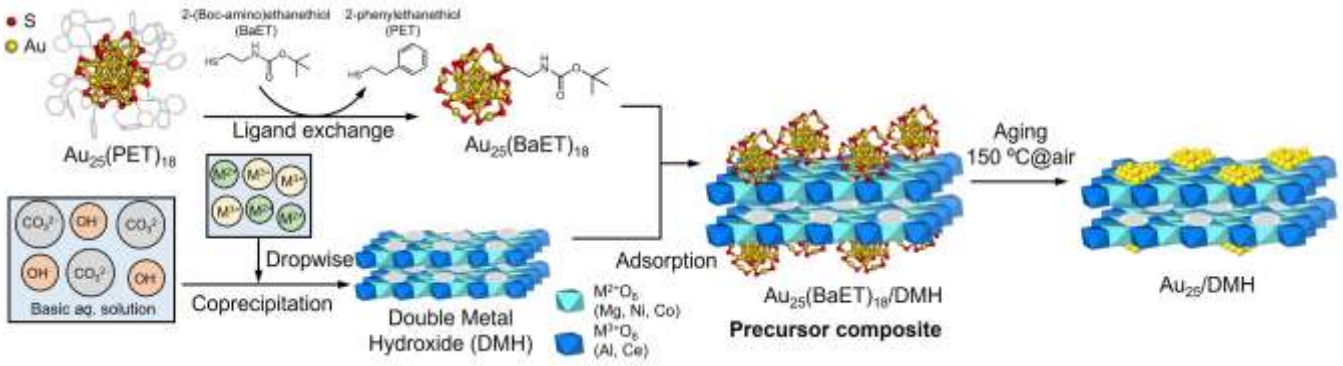

Scheme 2 Schematic illustration of procedure of synthesizing Au_{25}/DMH.

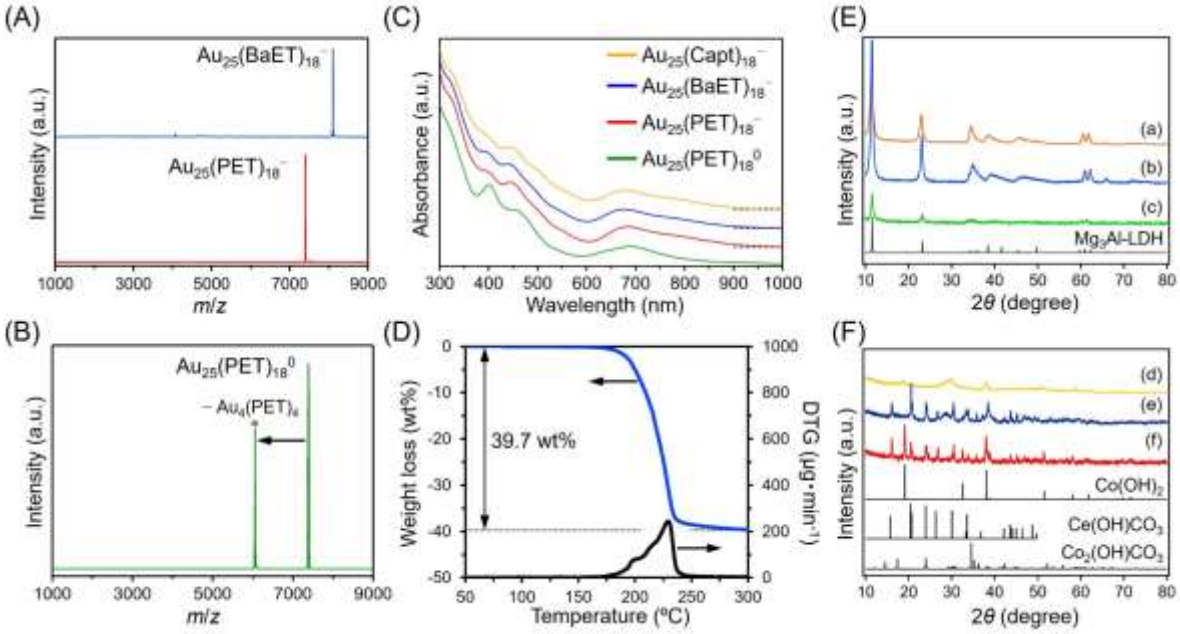

Fig. 1 (A) Negative-ion ESI mass spectra of $Au_{25}(BaET)_{18}^-$ and $Au_{25}(PET)_{18}^-$. (B) Negative-ion MALDI mass spectra of $Au_{25}(PET)_{18}^0$. (C) UV-vis absorption spectra of $Au_{25}(SR)_{18}^{-/0}$. (D) Thermogravimetric analysis of $Au_{25}(BaET)_{18}^-$. PXRD patterns of (E) Al^{3+} or (F) Ce^{3+}-containing DMH. (a) Mg_3Al, (b) Ni_3Al, (c) Co_3Al, (d) Mg_3Ce, (e) Ni_3Ce, and (f) Co_3Ce.

exhibited the patterns assigned to $Co(OH)_2$, $Ce(OH)CO_3$, and $Co_2(OH)CO_3$, indicating the formation of double metal hydroxide structures.[43] The Ni_3Ce showed similar PXRD patterns with those of Co_3Ce. Therefore, we concluded that the double hydroxide structures were also obtained in the Ce^{3+}-containing supports. **Fig. S1** shows nitrogen absorption–desorption isotherms of the DMHs. Specific surface areas and pore volumes calculated using the Brunauer–Emmett–Teller (BET) theory are summarized in **Table S1**. All supports have moderate specific surface areas (~150 m^2/g), which depend on the divalent metal cations and decrease in the order of Ni > Mg > Co. The results also suggest that similar structures were formed in the DMHs regardless of the trivalent metal cations. Scanning electron microscopy (SEM) and energy dispersive X-ray spectroscopy (EDX) show that the Co_3Ce support had assembled sheet-like structures with the size of ~1 μm, similarly to the conventional DMH, and that Co, Ce and O elements were distributed throughout the support (**Fig. S2**).

Finally, $Au_{25}(BaET)_{18}^-$ and $Au_{25}(Capt)_{18}^-$ were loaded onto various DMHs suspended in toluene and MeOH, respectively (**Scheme 2**). Successful loading of 1 wt% of the clusters was confirmed by UV-vis absorption spectra of the cluster solution before and after loading (**Fig. S3** and **S4**). $Au_{25}(PET)_{18}^0$ was loaded by the impregnation-evaporation method because of low adsorption efficiency in toluene. The obtained composites $Au_{25}(SR)_{18}$/DMH were aged at *T* °C for *t* h. The resulting catalysts are hereafter denoted as $Au_{25}(SR)_{18}$/DMH-*T*-*t*.

The degree of ligand removal as a function of aging conditions and the supports was qualitatively evaluated by catalytic activity for aerobic oxidation of benzyl alcohol ($PhCH_2OH$, **1**) in toluene. Benzaldehyde (PhCHO, **2**) was obtained as the sole product as reported previously in non-polar solvents.[31, 44] No catalysis of untreated composite $Au_{25}(BaET)_{18}/Co_3Ce$ (entry 1) indicates that two components $Au_{25}(BaET)_{18}$ and Co_3Ce are not catalytically active. Entries 2–7 in **Table 1** show that the activity of $Au_{25}(BaET)_{18}/Co_3Ce$-150-*t* increased with the aging period *t* from 2 to 12 h and remained

Table 1 Catalytic oxidation of benzyl alcohol in toluene[a]

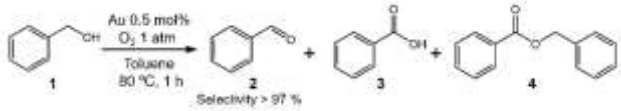

Entry	Catalyst [b]	*C* (%)[c]	TON[d]
1	$Au_{25}(BaET)_{18}/Co_3Ce$	0.0	–
2	$Au_{25}(BaET)_{18}/Co_3Ce$-150-2	2.4	5.0
3	$Au_{25}(BaET)_{18}/Co_3Ce$-150-4	10.1	20.1
4	$Au_{25}(BaET)_{18}/Co_3Ce$-150-8	71.8	144
5	$Au_{25}(BaET)_{18}/Co_3Ce$-150-12	75.6	159
6	$Au_{25}(BaET)_{18}/Co_3Ce$-150-20	80.6	162
7	$Au_{25}(BaET)_{18}/Co_3Ce$-150-30	79.5	160
8	$Au_{25}(BaET)_{18}/Mg_3Al$-150-12	0.0	–
9	$Au_{25}(BaET)_{18}/Ni_3Al$-150-12	34.5	72.5
10	$Au_{25}(BaET)_{18}/Co_3Al$-150-12	18.6	37.5
11	$Au_{25}(BaET)_{18}/Mg_3Ce$-150-12	3.0	6.2
12	$Au_{25}(BaET)_{18}/Ni_3Ce$-150-12	0.0	–
13	$Au_{25}(BaET)_{18}/Co_3Ce$-175-12	61.7	128
14	$Au_{25}(PET)_{18}/Co_3Ce$-150-12	76.1	152
15	$Au_{25}(Capt)_{18}/Co_3Ce$-150-12	52.1	105
16	$Au_{25}(Capt)_{18}/Co_3Ce$-150-20	74.6	150

Reaction conditions: **1** (102 μmol, 0.5 mol%), biphenyl (102 μmol), catalyst 10 mg, toluene 1 mL, 80 °C, 1 h, O_2 1 atm (balloon). [b]$Au_{25}(SR)_{18}$/DMH-*T*-*t* obtained by aging of $Au_{25}(SR)_{18}$/DMH at *T* (°C) for *t* (h). [c]Conversion of $PhCH_2OH$. [d]TON = [Mole of converted $PhCH_2OH$] / [Mole of gold (1 wt%)].

similar by increasing *t* to 20 and 30 h. These results suggest that the BaET ligands could be removed from $Au_{25}(BaET)_{18}/Co_3Ce$ by oxidative aging at 150 °C and became absent after 12 h. The removal of the BaET ligand at 150 °C was unexpected given that no weight loss was observed at 150 °C in the TG analysis of the $Au_{25}(BaET)_{18}$ powder (**Fig. 1D**). To confirm the desorption of BaET from $Au_{25}(BaET)_{18}/Co_3Ce$ at 150 °C, TG behaviour was compared between $Au_{25}(BaET)_{18}/Co_3Ce$ (5 wt%) and the Co_3Ce support (**Fig. S5**). The weight loss from $Au_{25}(BaET)_{18}/Co_3Ce$ was larger than that from the Co_3Ce reference (desorption of water and carbonate) after aging at 150 °C for 12 h, and the difference in the weight loss remained the same after heating at 500 °C. This result indicates that the BaET ligands were absent in $Au_{25}(BaET)_{18}/Co_3Ce$-150-12. Secondly, the effects of the support on the BaET desorption were investigated by comparing the catalysis of $Au_{25}(BaET)_{18}$/DMH-150-2. Entries 5 and 8–12 show that the Co_3Ce support gave the most active catalyst. These results indicate that Co_3Ce promotes desorption of thiolates from $Au_{25}(BaET)_{18}$ at 150 °C more efficiently than the other supports. $Au_{25}(BaET)_{18}/Co_3Ce$-150-30 (entry 7) exhibited comparable catalysis with $Au_{25}(BaET)_{18}/Co_3Ce$-150-12 (entry 5), while $Au_{25}(BaET)_{18}/Co_3Ce$-175-12 (entry 13) was less active than $Au_{25}(BaET)_{18}/Co_3Ce$-150-12 (entry 5). These results indicate that Au_{25} clusters are anchored strongly on Co_3Ce and that prolonged aging at 150 °C does not induce the aggregation of clusters. Finally, thermal desorption behaviour of various thiolates was compared. $Au_{25}(PET)_{18}/Co_3Ce$-150-12 and $Au_{25}(BaET)_{18}/Co_3Ce$-150-12 showed comparable activity (entries 4 and 14 in **Table 1**). On the other hand, $Au_{25}(Capt)_{18}/Co_3Ce$-150-12 exhibited lower activity than $Au_{25}(BaET)_{18}/Co_3Ce$-150-12 (entries 4 and 15), while $Au_{25}(Capt)_{18}/Co_3Ce$-150-20 showed comparable activity of $Au_{25}(BaET)_{18}/Co_3Ce$-150-12 (entries 4 and 16). These results suggest that various $Au_{25}(SR)_{18}$ can be used as starting materials of the catalysts, although more hydrophilic thiolate ligands require longer aging time. On the basis of the above results, we focused on the Au_{25} catalyst prepared by aging $Au_{25}(BaET)_{18}$ on Co_3Ce at 150 °C in the following experiments.

The structural change of $Au_{25}(BaET)_{18}$ on Co_3Ce during the aging was studied by Au L_3-edge XAFS measurement of the aged samples at room temperature. **Fig. 2A**, **2B**, and **S6A** show XANES spectra, Fourier transform of extended XAFS (FT-EXAFS) and EXAFS oscillations of the $Au_{25}(BaET)_{18}/Co_3Ce$-150-*t* samples with *t* = 0, 2, 4, 8, 12, 20, and 30, respectively.[45] XANES spectra of the untreated composite $Au_{25}(BaET)_{18}/Co_3Ce$ have a nearly featureless profile, whereas those of the aged samples gradually evolve peaked structures that can be assigned to metallic and oxidized Au at the white line region (**Fig. 2A**). The coordination numbers (*CN*s) and *r* values of Au–Au, Au–S, and Au–O bonds were determined by curve-fitting analyses of EXAFS and are summarized in **Table S2**. The time course of the *CN*s of each of the bonds (**Fig. 2C**) shows several features. Firstly, the *CN* value of the Au–S bond ($CN_{Au–S}$) monotonically reduced during aging for ≤8 h and became ~0 after aging for ≥12 h, suggesting that the BaET ligands were completely removed by oxidative aging for ≥12 h. This result is consistent with the results of the catalytic test (**Table 1**). Secondly, the *CN* value of the Au–Au bond ($CN_{Au–Au}$) gradually increased from 0.7 to ~6 during aging for 0–8 h and slightly reduced to 4–5 after 12 h. This time evolution of $CN_{Au–Au}$ is explained as follows by the structural change of the original $Au_{25}(BaET)_{18}$ (**Fig. 2D**). The $CN_{Au–Au}$ value before aging (0 h) was significantly underestimated with reference to that calculated from the crystal structure of $Au_{25}(PET)_{18}$ (3.3) because of the thermal effect on the EXAFS data, as we reported previously.[46] The $CN_{Au–Au}$ value at 8 h is comparable to those (6.0–6.5) estimated for hemispherical Au_{25}, suggesting the formation of Au_{25} clusters after complete removal of BaET. The $CN_{Au–Au}$ value after 12–30 h was slightly reduced to 4–5, suggesting the deformation of Au_{25} from hemispheres to flattened structures. A possible model structure is a monolayer of (111) plane of 25 Au atoms in face-centred cubic (fcc) structure whose $CN_{Au–Au}$ is estimated to

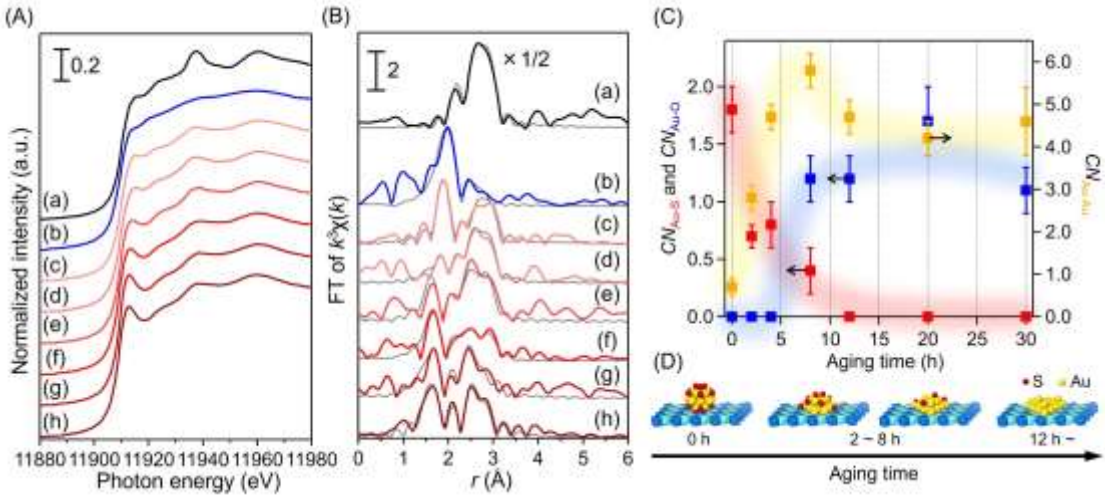

Fig. 2 (A) XANES spectra and (B) Fourier transform of EXAFS together with fitting curves of (a) Au foil, (b) $Au_{25}(BaET)_{18}/Co_3Ce$-150-*t* with *t* = (c) 2, (d) 4, (e) 8, (f) 12, (g) 20, and (h) 30, respectively. Solid line: raw data, dashed line: fitting data. (C) Time course of coordination numbers (*CN*s) of Au–S, Au–O, and Au–Au bonds estimated from curve-fitting analysis of the samples (Table S2). (D) Schematic representation of the oxidative aging processes of $Au_{25}(BaET)_{18}/Co_3Ce$ at 150 °C.

be 4.6. Thirdly, the *CN*s of the Au–O bond ($CN_{Au–O}$) exhibited behaviour that was the reverse of that of $CN_{Au–S}$ with the aging time, suggesting that the Au_{25} clusters are anchored on the oxygen atoms of Co_3Ce. We conclude from the time evolution of the *CN* values that the thermal-induced ligand removal from $Au_{25}(BaET)_{18}$ resulted in the formation of an Au_{25} cluster with a flattened structure anchored on Co_3Ce through strong Au–O bonds (**Fig. 2D**).

We examined the mechanistic insights of the low-temperature (150 °C) desorption of BaET from $Au_{25}(BaET)_{18}/Co_3Ce$. Firstly, the involvement of O_2 in the desorption was studied by XAFS measurement on $Au_{25}(BaET)_{18}/Co_3Ce$ after aging at 150 °C for 12 h *in vacuo* (**Fig. S7** and **S8**). The Au–S bond was clearly observed (**Table S3**), indicating that O_2 in air played an essential role in promoting desorption of BaET at 150 °C. Secondly, we tested the possibility that the CeO_2 impurity contained in our Co_3Ce promotes the desorption of thiolates according to the reports by Jin's and Barrabés's groups: $Au_{25}(SR)_{18}/CeO_2$ and $Au_{38}(SR)_{24}/CeO_2$ pretreated at 150 °C for >0.5 h catalyzed CO oxidation.[26, 32] XAFS analysis of $Au_{25}(BaET)_{18}/CeO_2$ after aging at 150 °C for 12 h (**Fig. S7** and **S8**) illustrated the presence of the Au–S bond (**Table S3**), indicating that the CeO_2 impurity, if present, did not play an important role in the desorption of thiolates. Based on these results, Co_3Ce promotes the thermal-induced oxidative desorption of thiolates in the presence of O_2 at low temperature.

Structure and oxidation catalysis of Au_{25}/Co_3Ce

In the following, we focus on further characterization of structures and catalysis of $Au_{25}(BaET)_{18}/Co_3Ce$-150-12, which will be abbreviated as Au_{25}/Co_3Ce. SEM images and aberration-corrected transmission electron microscope (ACTEM) images of Au_{25}/Co_3Ce are shown in **Fig. S9A** and **S9B**, respectively. The SEM images illustrate that the aged Co_3Ce support also had assembled sheet-like structures with the size of ~1 µm. The ACTEM images indicate the absence of large AuNPs although it was difficult to distinguish small Au clusters from DMH in the high-magnification images because of insufficient contrast. Therefore, Au_{25}/Co_3Ce was characterized by aberration-corrected high-angle annular dark field scanning transmission electron microscopy (AC-HAADF-STEM). **Fig. 3A** and **3B** compare typical AC-HAADF-STEM images and size distributions of untreated $Au_{25}(BaET)_{18}/Co_3Ce$ and aged Au_{25}/Co_3Ce, respectively. $Au_{25}(BaET)_{18}/Co_3Ce$ and Au_{25}/Co_3Ce exhibit monodisperse Au clusters with the average diameter of 1.5 ± 0.3 and 1.6 ± 0.4 nm, respectively. The cluster size of $Au_{25}(BaET)_{18}/Co_3Ce$ is slightly larger than that expected from the crystal structure of $Au_{25}(PET)_{18}$ due probably to electron beam induced damage.[47] We actually observed diffusion and fusion of the Au clusters during the imaging. Thus, it was difficult to estimate the exact number of the constituent Au atoms in Au_{25}/Co_3Ce. Nevertheless, nearly the same size distribution before and after aging combined with XAFS results leads us to conclude that atomically precise Au_{25} clusters were formed on Co_3Ce.

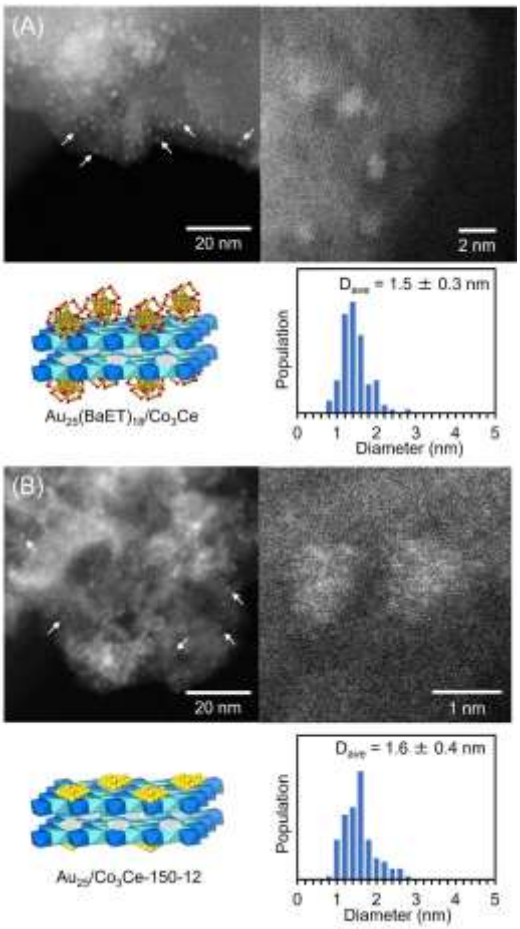

Fig. 3 AC-HAADF-STEM images and size distributions of Au clusters of (A) untreated $Au_{25}(BaET)_{18}/Co_3Ce$ and (B) aged Au_{25}/Co_3Ce. Some of the particles are indicated by the arrows.

High Au loading (1 wt%) in Au_{25}/Co_3Ce allowed us to probe the electronic structure by Au 4f XPS. The XP spectrum (**Fig. S10**) indicated that Au in Au_{25}/Co_3Ce was positively charged. XANES spectra of Au_{25}/Co_3Ce (**Fig. 2A**) showed a strong absorption peak in the white line region, which can be assigned to Au(I). Since almost all the constituent atoms in Au_{25}/Co_3Ce may interact with oxygen atoms in Co_3Ce as evidenced by XAFS results, the Au_{25} clusters are composed of positively charged Au atoms as in the case of AuNPs at the interface between basic supports.[3, 9, 10, 48-50]

The Au_{25}/Co_3Ce catalyst exhibited higher catalytic activity for aerobic oxidation of $PhCH_2OH$ in basic water than in toluene. **Table 2** summarizes the catalytic performances of Au_{25}/Co_3Ce for oxidation of $PhCH_2OH$ in water under various conditions. Au_{25}/Co_3Ce in basic (K_2CO_3) water at 30 °C in 0.5 h exhibited a high conversion (entry 1) comparable with that achieved at 80 °C for 1 h in toluene (entry 5 in **Table 1**). The catalytic performances of Au_{25}/Co_3Ce were further improved by using NaOH or KOH instead of K_2CO_3 (entries 2 and 3): 90% conversion with >99% selectivity to benzoic acid ($PhCO_2H$, **3**) was achieved. This activity originated from Au_{25} because Co_3Ce support itself showed negligible activity (entry 4). Then, the catalytic performance was tested by reducing the amount of catalyst to 0.1 mol%: 54.8% conversion with >97% selectivity was achieved

even at 30 min, and TOF reached 1097 h^{-1} at 30 °C (entry 5 and **Fig. 4A**). To the best of our knowledge, this obtained TOF value is among the highest reported for Au catalysts under similar conditions (**Table S4**).[27, 29, 31, 51-58] The catalytic conversion was completely stopped upon removing the catalyst by filtration (**Fig. 4A**), indicating that Au_{25}/Co_3Ce acted as a truly heterogeneous catalyst. The Au_{25}/Co_3Ce catalyst showed activity even under ambient air (entry 6). Moreover, the Au_{25}/Co_3Ce catalyst showed high durability in a recycling test while retaining activity and selectivity to $PhCO_2H$ till at least the third run (**Fig. 4B**).

Table 2 Catalytic oxidation of $PhCH_2OH$ in water

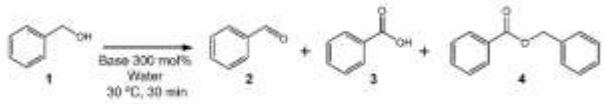

Entry	Base	C (%)[e]	Selectivity (%)			TON[f]	TOF (h^{-1})[g]
			2	3	4		
1[a]	K_2CO_3	79.2	2.4	62.5	35.1	159	318
2[a]	NaOH	90.8	1.8	98.2	0.0	181	363
3[a]	KOH	90.1	0.4	99.6	0.0	181	362
4[a, b]	KOH	2.5	48.9	51.1	0.0	—	—
5[c]	KOH	54.8	2.2	97.8	0.0	549	1097
6[d]	KOH	12.2	10.6	89.5	0.0	122	244

Au_{25}/Co_3Ce was used. [a]Reaction conditions: **1** (51 µmol, 0.5 mol%), catalyst 5 mg, base 300 mol%, water 1 mL, 30 °C, 30 min, O_2 1 atm (balloon). [b]Co_3Ce 5 mg was used instead of Au_{25}/Co_3Ce. [c]Reaction conditions: **1** (761 µmol, 0.1 mol%), catalyst 15 mg, base 300 mol%, water 15 mL, 30 °C, 30 min, O_2 1 atm (balloon). [d]Reaction conditions: **1** (761 µmol, 0.1 mol%), catalyst 15 mg, base 300 mol%, water 15 mL, 30 °C, 30 min, ambient air. [e]Conversion of $PhCH_2OH$. [f]TON = [Mole of converted $PhCH_2OH$] / [Mole of gold (1 wt%)]. [g]TOF = [TON] / [Reaction time (h)].

Mechanistic insights into oxidation catalysis

The mechanism of catalytic activity of Au_{25}/Co_3Ce was examined by kinetic studies. First, a large kinetic isotope effect of k_H/k_D = 12 was observed, where k_H (= 1.6 h^{-1}) and k_D (0.13 h^{-1}) are the rate constants of the oxidation of $PhCH_2OH$ and $PhCD_2OH$, respectively (**Fig. 5A**). This result suggests that the RDS is a C–D bond cleavage, that is, a hydride elimination step

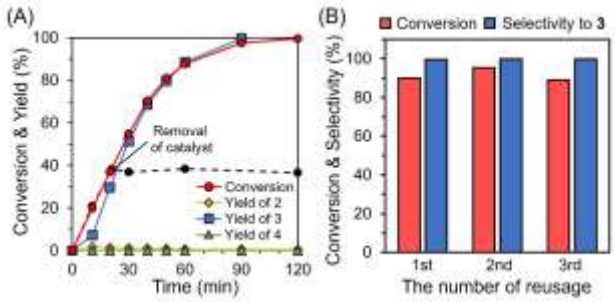

Fig. 4 (A) Time course of the conversion and yield for oxidation of $PhCH_2OH$ catalyzed by Au_{25}/Co_3Ce. Black dots represent the conversion after removing the catalyst by filtration. (B) Conversion and selectivity in recycling. Reaction conditions: (A) Au 0.1 mol%, KOH 300 mol%, water, 30 °C, O_2 1 atm or air; (B) Au 0.5 mol%, KOH 300 mol%, water, 30 °C, O_2 1 atm.

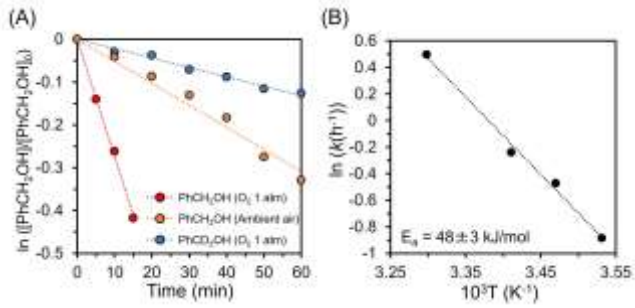

Fig. 5 (A) Kinetic experiments, and (B) Arrhenius plots over Au_{25}/Co_3Ce pretreated at 150 °C for 12 h. Reaction conditions: Au 0.1 mol% (A, C, and D) or 0.5 mol% (B), KOH 300 mol%, water, 30 °C, O_2 1 atm or ambient air.

from the α-carbon. The apparent activation energy (E_a) of the reaction was estimated to be 48 ± 3 kJ/mol from the Arrhenius plot (**Fig. 5B** and **Fig. S11**). Next, we investigated the effect of O_2 pressure on the oxidation rates of $PhCH_2OH$ by comparing the activities under 1 atm of O_2 and ambient air. The oxidation rates were significantly different: k_{O2}/k_{air} = 5.4, where k_{air} = 0.31 h^{-1} (**Fig. 5A**). Moreover, the conversion in ambient air linearly increased even at a low concentration of $PhCH_2OH$ (**Fig. S12**), indicating that the reaction rate is zeroth order with respect to $PhCH_2OH$. This result implies that the diffusion or activation of O_2 becomes the RDS at low O_2 partial pressure.

The overall rate of the consecutive oxidation reaction in water ($PhCH_2OH$ → PhCHO → $PhCO_2H$) is determined by the first step since the yield of PhCHO remained low throughout the reaction (**Fig. 4A**). It has been reported that positively charged AuNPs can abstract hydride (H^-) from benzyl alcohol, followed by removal of H^- by O_2[59-61] and that hydrogen atoms preadsorbed on positively charged Au clusters can activate O_2 to form hydroperoxide (HOO^-).[62] These reports led us to propose the following mechanism for the oxidation of $PhCH_2OH$ to PhCHO catalyzed by Au_{25}/Co_3Ce in water (**Scheme 3**). Firstly, the alkoxide ($PhCH_2O^-$) formed by the deprotonation of $PhCH_2OH$ with base adsorbs onto positively charged Au_{25} (**step**

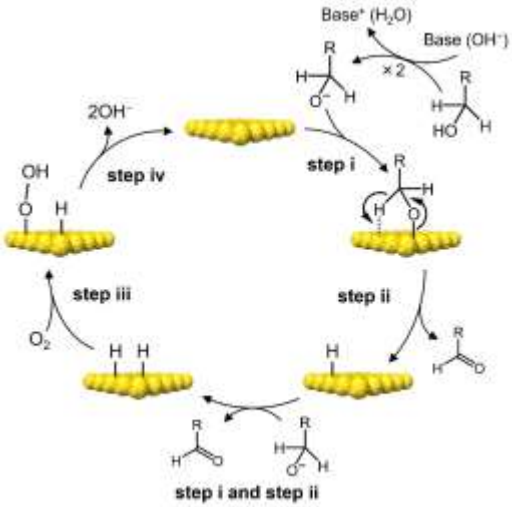

Scheme 3 Proposed pathway of the first oxidation step of $PhCH_2OH$ to PhCHO on Au_{25}/Co_3Ce in water. Steps ii and iii are rate determining steps under 1 atm and low partial pressure of O_2, respectively.

i). Then, the H^- is abstracted from the α-carbon of the adsorbed alkoxide by positively charged Au_{25}, to produce PhCHO (**step ii**). Finally, the Au_{25} catalyst is regenerated by desorbing H^- by dissolved O_2 in the form HOO^- (**step iii**) which subsequently reacted with H^- to form OH^- (**step iv**). **Steps ii** and **iii** correspond to the RDSs under 1 atm of O_2 and ambient air, respectively. PhCHO thus produced is swiftly oxidized to $PhCO_2H$ according to the pathway shown in **Scheme S1**. Since this oxidation step did not proceed in toluene (Table 1) but in water (Table 2), we propose that $PhCO_2H$ is formed by nucleophilic attack of water to the α-carbon of PhCHO adsorbed on Au_{25}. The role of O_2 in this oxidation step is similar to that in **Scheme 3**.

Recently, we reported that H^- abstraction from the α-carbon of $PhCH_2OH$ also corresponds to the RDS of the oxidation by negatively charged Au_{24} clusters stabilized by PVP ($k_H/k_D = 4.1$, $E_a = 56 \pm 3$ kJ/mol) under 1 atm of O_2.[63] On the other hand, the dependence of O_2 partial pressure on the reaction rates by Au_{24}:PVP ($k_{O2}/k_{air} = 1.4$) and Au_{25}/Co_3Ce ($k_{O2}/k_{air} = 5.4$) suggests that the H^- elimination by gold followed by removal of H^- on gold by O_2 or the abstraction of H^- from α-carbon of $PhCH_2OH$ by adsorbed O_2 are involved in the alcohol oxidation by Au_{25}/Co_3Ce or Au_{24}:PVP, respectively, under ambient air.

Conclusions

In this study, atomically precise bare Au_{25} clusters were successfully immobilized on the Co_3Ce support by oxidative aging of $Au_{25}(BaET)_{18}$ at a low temperature (150 °C) for a long time (12 h). This finding indicates that the Co_3Ce support promotes the RS desorption with the help of O_2. The Au_{25} clusters retained their original size even after aging at 150 °C for 30 h, but took flattened structures due to strong interaction with the Co_3Ce support through the Au–O bonds. The Au_{25}/Co_3Ce catalyst oxidized benzyl alcohol efficiently and selectively to benzoic acid (selectivity >97%) in water under ambient conditions: the TOF value (1097 h^{-1}) is among the highest reported for Au catalysts under similar conditions. The abstraction of hydride from the α-carbon of the adsorbed alkoxide by Au_{25} is the rate-determining step. The low-temperature aging of predefined $Au_x(SR)_y$ on Co_3Ce paves the way for the synthesis of atomically precise, heterogeneous Au_x clusters catalysts, which may exhibit novel catalysis in a variety of reactions.

Experimental

All methods are summarized in the Supplementary Information file.

Author Contributions

Shinya Masuda synthesized the clusters and catalysts, performed characterizations and catalytic reactions, and wrote the manuscript. Shinjiro Takano synthesized the cluster precursors and clusters. Seiji Yamazoe helped with measuring and analyzing XAFS data. Tatsuya Tsukuda supervised the project and wrote the manuscript. The manuscript was written through discussions among all authors, all of whom approved the final version.

Conflicts of interest

There are no conflicts to declare.

Acknowledgements

The authors thank Prof. Eiichi Nakamura, Prof. Koji Harano, and Dr. Takayuki Nakamuro (the University of Tokyo) for providing access to the SEM and ACTEM apparatus. This research was financially supported by JST, CREST (grant no. JPMJCR20B2), the Elements Strategy Initiative for Catalysts & Batteries (ESICB), the University of Tokyo Advanced Characterization Nanotechnology Platform in the Nanotechnology Platform Project sponsored by the Ministry of Education, Culture, Sports, Science and Technology (MEXT), Japan (Project No. JPMXP09A20UT0024 and JPMXP09A21UT0168) and a Grant-in-Aid for Scientific Research (A) (Grant No. 20H00370), for Research Activity Start-up (Grant No. 20K22548), and for Early-Career Scientists (Grant No. 21K14476) from the Japan Society for the Promotion of Science (JSPS). The synchrotron radiation experiments were performed with the approval of the Japan Synchrotron Radiation Research Institute (JASRI) as 2020A0672 and 2021A1200.

Notes and references

1. M. Haruta, T. Kobayashi, H. Sano and N. Yamada, *Chem. Lett.*, 1987, **16**, 405–408.
2. M. Sankar, Q. He, R. V. Engel, M. A. Sainna, A. J. Logsdail, A. Roldan, D. J. Willock, N. Agarwal, C. J. Kiely and G. J. Hutchings, *Chem. Rev.*, 2020, **120**, 3890–3938.
3. T. Ishida, T. Murayama, A. Taketoshi and M. Haruta, *Chem. Rev.*, 2020, **120**, 464–525.
4. T. Takei, T. Akita, I. Nakamura, T. Fujitani, M. Okumura, K. Okazaki, J. Huang, T. Ishida and M. Haruta, *Advances in Catalysis, Gates, B. C., Jentoft, F. C., Eds. Academic Press:*, 2012, **55**, 1–126.
5. A. Corma and H. Garcia, *Chem. Soc. Rev.*, 2008, **37**, 2096–2126.
6. H. Tsunoyama, H. Sakurai and T. Tsukuda, *Chem. Phys. Lett.*, 2006, **429**, 528–532.
7. M. Haruta, S. Tsubota, T. Kobayashi, H. Kageyama, M. J. Genet and B. Delmon, *J. Catal.*, 1993, **144**, 175–192.
8. T. Fujitani and I. Nakamura, *Angew. Chem. Int. Ed.*, 2011, **50**, 10144–10147.
9. S. Minicò, S. Scirè, C. Crisafulli, A. M. Visco and S. Galvagno, *Catal. Lett.*, 1997, **47**, 273–276.
10. J. Guzman and B. C. Gates, *J. Am. Chem. Soc.*, 2004, **126**, 2672–2673.
11. J. Zhang, H. Wang, L. Wang, S. Ali, C. Wang, L. Wang, X. Meng, B. Li, D. S. Su and F. S. Xiao, *J. Am. Chem. Soc.*, 2019, **141**, 2975–2983.
12. M. Haruta, *Faraday Discuss.*, 2011, **152**, 11–32.
13. R. Jin, C. Zeng, M. Zhou and Y. Chen, *Chem. Rev.*, 2016, **116**, 10346–10413.
14. S. Yamazoe, K. Koyasu and T. Tsukuda, *Acc. Chem. Res.*, 2014, **47**, 816–824.

15. I. Chakraborty and T. Pradeep, *Chem. Rev.*, 2017, **117**, 8208–8271.
16. L. Liu and A. Corma, *Chem. Rev.*, 2018, **118**, 4981–5079.
17. S. Takano and T. Tsukuda, *J. Am. Chem. Soc.*, 2021, **143**, 1683–1698.
18. B. Yoon, H. Häkkinen, U. Landman, A. S. Wörz, J.-M. Antonietti, S. Abbet, K. Judai and U. Heiz, *Science*, 2005, **307**, 403–407.
19. W. T. Wallace and R. L. Whetten, *J. Am. Chem. Soc.*, 2002, **124**, 7499–7505.
20. L. D. Socaciu, J. Hagen, T. M. Bernhardt, L. Wöste, U. Heiz, H. Häkkinen and U. Landman, *J. Am. Chem. Soc.*, 2003, **125**, 10437–10445.
21. T. Kawawaki, Y. Kataoka, M. Hirata, Y. Iwamatsu, S. Hossain and Y. Negishi, *Nanoscale Horiz.*, 2021, **6**, 409–448.
22. V. Sudheeshkumar, K. O. Sulaiman and R. W. J. Scott, *Nanoscale Adv.*, 2020, **2**, 55–69.
23. S. Pollitt, V. Truttmann, T. Haunold, C. Garcia, W. Olszewski, J. Llorca, N. Barrabés and G. Rupprechter, *ACS Catal.*, 2020, **10**, 6144–6148.
24. A. Longo, E. J. J. de Boed, N. Mammen, M. van der Linden, K. Honkala, H. Häkkinen, P. E. de Jongh and B. Donoeva, *Chem. Eur.*, 2020, **26**, 7051–7058.
25. X. Nie, H. Qian, Q. Ge, H. Xu and R. Jin, *ACS Nano*, 2012, **6**, 6014–6022.
26. C. Liu, J. Zhang, J. Huang, C. Zhang, F. Hong, Y. Zhou, G. Li and M. Haruta, *ChemSusChem*, 2017, **10**, 1976–1980.
27. T. Yoskamtorn, S. Yamazoe, R. Takahata, J.-i. Nishigaki, A. Thivasasith, J. Limtrakul and T. Tsukuda, *ACS Catal.*, 2014, **4**, 3696–3700.
28. S. Xie, H. Tsunoyama, W. Kurashige, Y. Negishi and T. Tsukuda, *ACS Catal.*, 2012, **2**, 1519–1523.
29. S. Yamazoe, T. Yoskamtorn, S. Takano, S. Yadnum, J. Limtrakul and T. Tsukuda, *Chem. Rec.*, 2016, **16**, 2338–2348.
30. W. Kurashige, R. Hayashi, K. Wakamatsu, Y. Kataoka, S. Hossain, A. Iwase, A. Kudo, S. Yamazoe and Y. Negishi, *ACS Appl. Energy Mater.*, 2019, **2**, 4175–4187.
31. Y. Xu, J. Li, J. Zhou, Y. Liu, Z. Wei and H. Zhang, *J. Catal.*, 2020, **389**, 409–420.
32. S. Wang, S. Yin, G. Chen, L. Li and H. Zhang, *Catal. Sci. Technol.*, 2016, **6**, 4090–4104.
33. J. Fang, J. Li, B. Zhang, X. Yuan, H. Asakura, T. Tanaka, K. Teramura, J. Xie and N. Yan, *Nanoscale*, 2015, **7**, 6325–6333.
34. T. Kawawaki, Y. Kataoka, M. Hirata, Y. Akinaga, R. Takahata, K. Wakamatsu, Y. Fujiki, M. Kataoka, S. Kikkawa, A. S. Alotabi, S. Hossain, D. J. Osborn, T. Teranishi, G. G. Andersson, G. F. Metha, S. Yamazoe and Y. Negishi, *Angew. Chem. Int. Ed.*, 2021, **60**, 21340–21350.
35. M. Haruta, N. Yamada, T. Kobayashi and S. Iijima, *J. Catal.*, 1989, **115**, 301–309.
36. J. Lu, B. Fu, M. C. Kung, G. Xiao, J. W. Elam, H. H. Kung and P. C. Stair, *Science*, 2012, **335**, 1205–1208.
37. X. Kang, H. Chong and M. Zhu, *Nanoscale*, 2018, **10**, 10758-10834.
38. T. Mitsudome, A. Noujima, T. Mizugaki, K. Jitsukawa and K. Kaneda, *Adv. Synth. Catal.*, 2009, **351**, 1890–1896.
39. W. Fang, J. Chen, Q. Zhang, W. Deng and Y. Wang, *Chem. Eur.*, 2011, **17**, 1247–1256.
40. B. M. Choudary, M. L. Kantam, A. Rahman, C. V. Reddy and K. K. Rao, *Angew. Chem. Int. Ed.*, 2001, **40**, 763–766.
41. M. A. Tofanelli, K. Salorinne, T. W. Ni, S. Malola, B. Newell, B. Phillips, H. Häkkinen and C. J. Ackerson, *Chem. Sci.*, 2016, **7**, 1882–1890.
42. S. Kumar and R. Jin, *Nanoscale*, 2012, **4**, 4222–4227.
43. E. Lucchini and C. Schmid, *J. Mater. Sci. Lett.*, 1988, **7**, 523–524.
44. S. Rautiainen, O. Simakova, H. Guo, A.-R. Leino, K. Kordás, D. Murzin, M. Leskelä and T. Repo, *Appl. Catal. A: Gen.*, 2014, **485**, 202–206.
45. H. Asakura, S. Yamazoe, T. Misumi, A. Fujita, T. Tsukuda and T. Tanaka, *Radiat. Phys. Chem.* , 2020, **175**, 108270.
46. S. Yamazoe and T. Tsukuda, *Bull. Chem. Soc. Jpn.*, 2018, **92**, 193–204.
47. M. Zhu, C. M. Aikens, F. J. Hollander, G. C. Schatz and R. Jin, *J. Am. Chem. Soc.*, 2008, **130**, 5883–5885.
48. M. Wang, F. Wang, J. Ma, M. Li, Z. Zhang, Y. Wang, X. Zhang and J. Xu, *Chem. Commun.*, 2014, **50**, 292–294.
49. J. H. Carter, P. M. Shah, E. Nowicka, S. J. Freakley, D. J. Morgan, S. Golunski and G. J. Hutchings, *Front. Chem*, 2019, **7**, 443.
50. H. Tang, Y. Su, B. Zhang, A. F. Lee, M. A. Isaacs, K. Wilson, L. Li, Y. Ren, J. Huang, M. Haruta, B. Qiao, X. Liu, C. Jin, D. Su, J. Wang and T. Zhang, *Sci. Adv.*, 2017, **3**, e1700231.
51. S. Wang, J. Wang, Q. Zhao, D. Li, J.-Q. Wang, M. Cho, H. Cho, O. Terasaki, S. Chen and Y. Wan, *ACS Catal.*, 2015, **5**, 797–802.
52. S. Wang, Q. Zhao, H. Wei, J.-Q. Wang, M. Cho, H. S. Cho, O. Terasaki and Y. Wan, *J. Am. Chem. Soc.*, 2013, **135**, 11849–11860.
53. H. Tsunoyama, H. Sakurai, Y. Negishi and T. Tsukuda, *J. Am. Chem. Soc.*, 2005, **127**, 9374–9375.
54. L. Wolski, G. Nowaczyk, S. Jurga and M. Ziolek, *Catalysts*, 2021, **11**, 641.
55. P. Liu, V. Degirmenci and E. J. M. Hensen, *J. Catal.*, 2014, **313**, 80–91.
56. L. Lei, H. Liu, Z. Wu, Z. Qin, G. Wang, J. Ma, L. Luo, W. Fan and J. Wang, *ACS Appl. Nano Mater.*, 2019, **2**, 5214–5223.
57. T. Wang, X. Yuan, S. Li, L. Zeng and J. Gong, *Nanoscale*, 2015, **7**, 7593–7602.
58. Z. Wang, C. Xu and H. Wang, *Catal. Lett.*, 2014, **144**, 1919–1929.
59. M. Conte, H. Miyamura, S. Kobayashi and V. Chechik, *J. Am. Chem. Soc.*, 2009, **131**, 7189–7196.
60. A. Abad, A. Corma and H. García, *Chem. Eur.*, 2008, **14**, 212–222.
61. A. Mahdavi-Shakib, J. Sempel, L. Babb, A. Oza, M. Hoffman, T. N. Whittaker, B. D. Chandler and R. N. Austin, *ACS Catal.*, 2020, **10**, 10207–10215.
62. S. M. Lang, T. M. Bernhardt, R. N. Barnett, B. Yoon and U. Landman, *J. Am. Chem. Soc.*, 2009, **131**, 8939–8951.
63. S. Hasegawa, S. Takano, K. Harano and T. Tsukuda, *JACS Au*, 2021, **1**, 660–668.